Physics of the Earth and Planetary Interiors 261 (2016) 196–206

Contents lists available at ScienceDirect

Physics of the Earth and Planetary Interiors

journal homepage: www.elsevier.com/locate/pepi

The phase diagram of NiSi under the conditions of small planetary interiors

David P. Dobson [a,*], Simon A. Hunt [a], Jabraan Ahmed [a], Oliver T. Lord [b], Elizabeth T.H. Wann [a], James Santangeli [a], Ian G. Wood [a], Lidunka Vočadlo [a], Andrew M. Walker [b,1], Andrew R. Thomson [a,b], Marzena A. Baron [b,c], Hans J. Mueller [d], Christian Lathe [d], Matthew Whitaker [e], Guillaume Morard [f], Mohamed Mezouar [g]

[a] Department of Earth Sciences, University College London, Gower Street, London WC1E 6BT, UK
[b] School of Earth Sciences, University of Bristol, Wills Memorial Building, Queen's Road, Bristol BS8 1RJ, UK
[c] Centre for Earth Evolution and Dynamics (CEED), University of Oslo, P.O. Box 1028 Blindern, N-0315 Oslo, Norway
[d] GFZ German Research Centre for Geosciences, Telegraphenberg, D-14473 Potsdam, Germany
[e] Mineral Physics Institute, Department of Earth and Space Sciences, Stony Brook University, Stony Brook, New York, USA
[f] Institut de Minéralogie, de Physique des Matériaux, et de Cosmochimie (IMPMC), Sorbonne Universités – UPMC, UMR CNRS 7590, Muséum National d'Histoire Naturelle, IRD UMR 206, F-75005 Paris, France
[g] European Synchrotron Radiation Facility, Grenoble, France

ARTICLE INFO

Article history:
Received 10 August 2016
Received in revised form 11 October 2016
Accepted 12 October 2016
Available online 14 October 2016

ABSTRACT

The phase diagram of NiSi has been determined using *in situ* synchrotron X-ray powder diffraction multi-anvil experiments to 19 GPa, with further preliminary results in the laser-heated diamond cell reported to 60 GPa. The low-pressure MnP-structured phase transforms to two different high-pressure phases depending on the temperature: the ε-FeSi structure is stable at temperatures above ~1100 K and a previously reported distorted-CuTi structure (with *Pmmn* symmetry) is stable at lower temperature. The invariant point is located at 12.8 ± 0.2 GPa and 1100 ± 20 K. At higher pressures, ε-FeSi-structured NiSi transforms to the CsCl structure with CsCl-NiSi as the liquidus phase above 30 GPa. The Clapeyron slope of this transition is −67 MPa/K. The phase boundary between the ε-FeSi and *Pmmn* structured phases is nearly pressure independent implying there will be a second sub-solidus invariant point between CsCl, ε-FeSi and *Pmmn* structures at higher pressure than attained in this study. In addition to these stable phases, the MnP structure was observed to spontaneously transform at room temperature to a new orthorhombic structure (also with *Pnma* symmetry) which had been detailed in previous *ab initio* simulations. This new phase of NiSi is shown here to be metastable.

1. Introduction

We have known for over half a century (Birch, 1964) that the core of the Earth has a density which is somewhat lower than that of pure iron under similar conditions of pressure and temperature; this density deficit is postulated to be due to the presence of approximately 10 wt.% of a light alloying element (or elements). Cosmochemical arguments suggest that the core of the Earth also contains 5 wt.% or more nickel and some iron meteorites contain up to 20 wt.% nickel, although nickel has been largely ignored in studies of core materials. Recent experimental and *ab initio* simulation studies, however, have shown that simple mixtures of iron and light elements cannot be reconciled with the seismic velocities of the core at the correct core densities (see e.g. Vočadlo, 2007; Antonangeli et al., 2010) prompting interest in the role of nickel in the core (Kantor et al., 2007; Kuwayama et al., 2008; Martorell et al., 2013). Silicon is thought to be a major light element component in the core of terrestrial planets, along with sulphur (e.g. Malavergne et al., 2010; Deng et al., 2013; Chabot et al., 2014) so iron silicide and nickel silicide are important end-member components for understanding the chemical and physical properties of planetary cores. In the extensively studied FeSi system the ε-FeSi structure that is stable at ambient conditions transforms to a CsCl-structured phase at ~20 GPa, which remains stable to pressures greater than those in the core of the Earth (Vočadlo et al., 1999; Dobson et al., 2002, 2003; Dubrovinsky et al., 2003; Caracas and Wentzcovitch, 2004; Lord et al., 2010; Zhang and Oganov, 2010; Fischer et al., 2013; Geballe and Jeanloz, 2012).

* Corresponding author.
E-mail address: d.dobson@ucl.ac.uk (D.P. Dobson).
[1] Now at: School of Earth and Environment, University of Leeds, Leeds LS2 9JT, UK.

http://dx.doi.org/10.1016/j.pepi.2016.10.005
0031-9201/

Static *ab initio* simulations of NiSi (Vočadlo et al., 2012) revealed significantly more complex phase relations under compression than those observed in FeSi. In that study it was reported that there were 4 different stable structures under compression before NiSi takes on the CsCl structure (space group $Pm\bar{3}m$, also known as B2 in the Strukturbericht notation) at ~250 GPa. As expected, the MnP-structured (*Pnma*, B31) phase was determined to be the most stable form of NiSi at atmospheric pressure but, at a simulation pressure of ~23 GPa, NiSi with the γ-CuTi (*P*4/*nmm*, B11) structure became the most stable phase. Two orthorhombic structures were determined to become stable at higher pressures, the first with space group *Pbnm* and the second being the FeB structure (*Pnma*, B27). NiSi with the ε-FeSi ($P2_13$, B20) structure was not found to be stable at any pressure, but the energy differences between this and the other phases were only a few meV per atom. The stable zero-Kelvin structures were subsequently confirmed by Gavryushkin et al. (2015) using *ab initio*-based structure prediction software. A subsequent experimental study by Lord et al. (2012), in which synchrotron X-ray diffraction was used to examine samples quenched from high-temperature in the laser-heated diamond-anvil-cell, confirmed the CsCl-structured phase of NiSi at pressures above 46 GPa and temperatures above 1900 K, and also determined the ε-FeSi-structured phase to be the thermodynamically most stable structure at pressures between about 12.5 and 46 GPa and temperatures above 1550 K. In addition, some very weak reflections in the X-ray diffraction patterns were observed that were consistent with other structures predicted to be stable in the *ab initio* study. It was thought that these were possibly stable phases at lower temperatures, produced at the edges of the laser heated spot or during temperature quenching prior to X-ray diffraction. Laser-heated diamond-anvil cells are not amenable to studies below ~1500 K so we performed preliminary multi-anvil experiments to determine whether the γ-CuTi structured phase, predicted to become stable at a simulated pressure of ~23 GPa, was indeed the stable structure of NiSi at high-pressure and moderate temperature. At 17.5 GPa and 1000–1200 K an orthorhombically-distorted (*Pmmn*) version of the γ-CuTi structure (hereafter termed the distorted-CuTi structure) was observed in quenched samples, coexisting with ε-FeSi structured NiSi (hereafter termed the ε-FeSi structure; Wood et al., 2013). This material had a different crystal structure from the orthorhombically distorted structure with space group *Pbma* considered in the earlier *ab initio* simulations of Vočadlo et al. (2012). In the case of the simulations, the distortion was along the diagonals of the a-b plane of the γ -CuTi phase, requiring an axial transformation of $a_0 \approx b_0 \approx \sqrt{2}a$, where a_0 and b_0 are the axes of the orthorhombic phase, whereas the experimentally observed phase had a distortion along the a and b axes of the tetragonal γ-CuTi phase. Static *ab initio* simulations have subsequently shown this distorted-CuTi structure to be more stable than the γ-CuTi structure from which it is derived at all positive pressures, with the predicted transition from the low pressure MnP (*Pnma*) phase to the distorted-CuTi structure occurring at 21 GPa (Wood et al., 2013). Simulations indicate that this distortion increases with decreasing lattice volume, suggesting that the tetragonal structure might become stable at elevated temperature. The equation of state and distortion of this phase has subsequently been experimentally determined to be in excellent agreement with the simulations to at least 45 GPa (Lord et al., 2015). It is clear from these earlier studies that the phase diagram of NiSi under moderate conditions of pressure and temperature is complex, with both pressure- and temperature-induced transitions between quite distinct structure-types and further ferroelastic distortions of the CuTi structure possible. We report here, therefore, the sub-solidus P-T phase diagram of the NiSi system up to 19 GPa and 1773 K by *in situ*, multi-anvil based, synchrotron X-ray diffraction studies at simultaneous high pressure and high temperature, along with preliminary results to 60 GPa from *in situ* laser-heated diamond-anvil cell experiments also using synchrotron X-ray diffraction. The melting curve of NiSi has already been presented up to 70 GPa (Lord et al., 2014), based in part on the results of the *in situ* laser-heated diamond anvil cell experiments reported here.

2. Methods

The starting material for all experiments was produced by arc-melting a stoichiometric mixture of Ni and Si and was the same as the starting material used in our previous studies (Lord et al., 2012, 2014; Wood et al., 2013). Laboratory X-ray diffraction at UCL confirmed that the material had the expected MnP structure while electron-probe analyses confirmed that the bulk of the sample was very nearly stoichiometric, with composition $Ni_{49.84(6)}Si_{50.16(6)}$. A trace amount of material with approximately Ni_3Si_2 composition was observed on the grain-boundaries of the starting material in the electron probe analyses. Laboratory X-ray diffraction indicates that this material is in fact an intergrowth of MnP structured NiSi and δ-Ni_2Si that is too fine to be resolved by the microprobe, thus yielding an average composition of Ni_3Si_2 (see Lord et al., 2012 for more details).

Two series of *in situ* multi-anvil press experiments were performed to determine the phase diagram of NiSi. The cells used for both sets of *in situ* experiments are drawn in Fig. 1. Temperature was measured in all multi-anvil experiments using W-Re (3–25) thermocouples; in both *in situ* cases, the diffraction volume was within 250 μm of the thermocouple junction.

The first set of *in situ* experiments, performed at beamline X17b2 of the National Synchrotron Light Source (NSLS), Brookhaven National Laboratory, USA, used a 250 tonne DIA-type multi anvil press with a 6 mm baked pyrophyllite cube compressed with 4 mm sintered-diamond anvils (Fig. 1a). The furnace was a graphite cylinder, with Al_2O_3 thermal insulation between the furnace and cube. A hexagonal BN cylinder, placed inside the furnace, contained thin-walled corundum capsules, one with a fine-grained mixture of NaCl and BN as a pressure standard, and the other with a finely-ground NiSi sample. Energy-dispersive X-ray diffraction patterns were collected at a 2θ angle of 6.5 degrees, alternating with sample imaging using a fluorescent YAG crystal and low-light video camera-microscope system, described elsewhere (Dobson et al., 2010). At each temperature, a diffraction pattern was recorded, first from the NaCl/BN pressure standard, then from the sample; finally, the incident beam slits were removed and an image was taken of the sample. The incident and diffracted beams were collimated to 50 by 50 μm and diffraction exposure times were approximately 5 min for phase identification.

The second set of *in situ* experiments was performed at the DORIS synchrotron, DESY, Hamburg, Germany, on MAX200x, a 1750 tonne DIA-type press with a 6–8 double-stage geometry. Chromium-doped MgO octahedra of 10 mm edge length were compressed by 5 mm truncated WC anvils (Fig. 1b). The furnace comprised a 25 μm thick Inconel foil, with 0.5 mm of ZrO_2 thermal insulation between the furnace and octahedron. The zirconia was replaced with MgO in the central 2 mm which contained the X-ray path. MgO capsules, containing a mixture of NiSi and NaCl (as the pressure standard), were placed directly inside the furnace. At each temperature X-ray diffraction patterns were collected from the NiSi/NaCl mixture but imaging was not possible in these experiments. Energy dispersive X-ray diffraction was performed using incident and diffracted beams collimated to 0.5 mm × 0.5 mm at a 2θ angle of 3.2 degrees and diffraction exposure times were approximately 5 min.

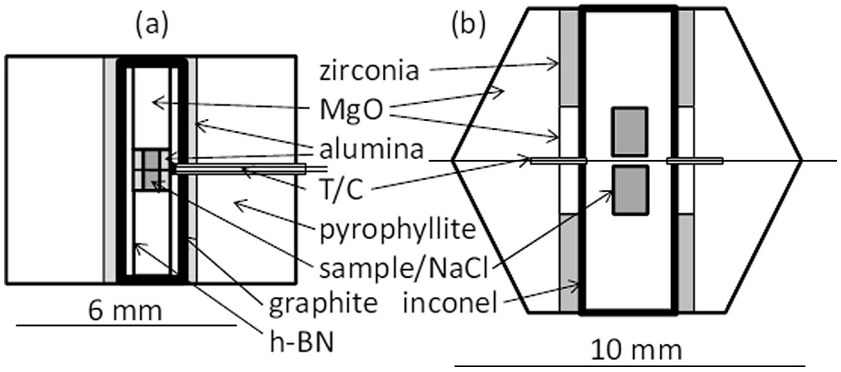

Fig. 1. Multi-anvil cells for *in situ* experiments at (a) NSLS and (b) DORIS.

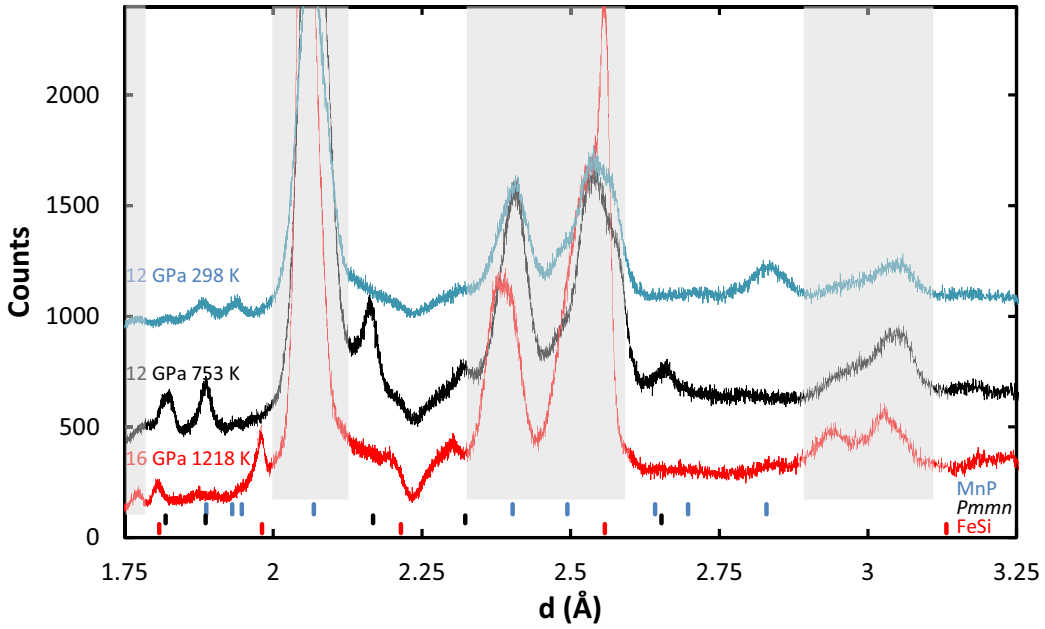

Fig. 2. Representative diffraction patterns from DORIS experiments collected at 12 GPa, 298 K (top); 12 GPa, 753 K (middle); 16 GPa, 1218 K (bottom). Tick marks show positions of reflections from NiSi Phases, from top to bottom: MnP, distorted-CuTi, ε-FeSi. Regions of the patterns marked in grey are dominated by reflections from the MgO pressure medium and Inconel furnace. Characteristic reflections used to identify the phases of NiSi were: for MnP, 101 (2.830 Å), 121 (1.931 Å) and 220 (1.888 Å); for ε-FeSi, 200 (2.214 Å, which appears as a shoulder on the MgO 200 reflection), 210 (1.981 Å) and 211 (1.808 Å); for distorted-CuTi (*Pmmn*), 101 (2.653 Å), 002 (2.323 Å), 110 (2.168 Å), 102 (1.886 Å) and 012 (1.819 Å). The 111 reflection of the ε-FeSi phase (2.557 Å) is also clear but it overlaps with reflections from the pressure medium so was not considered to be diagnostic.

All multi-anvil press *in situ* experiments were performed by compression at room temperature to the desired end-load, followed by step-wise heating. Pressure was determined from the P-V-T equation of state of NaCl with the B1 structure (Decker, 1971). The main error in pressure comes from errors in fitting the NaCl diffraction pattern and is typically 0.1–0.2 GPa. Phase transitions were determined by the appearance of the following diagnostic reflections for the MnP (101, 121 and 220), ε-FeSi (200, 210 and 211) and *Pmmn* (101, 002, 110, 102 and 012) phases of NiSi (Fig. 2). In general, the reaction kinetics were very fast, with complete transformation from one phase to another in less than 20 min at even the lowest temperatures, with the exception of the distorted-CuTi to ε-FeSi phase boundary (see Section 3.2). Once an equilibrium phase boundary was crossed and the new phase produced, the pressure and temperature conditions were altered in order to reverse the reaction. The equilibrium phase boundaries were thus followed by repeatedly observing the forward and reverse reactions at small increments of pressure and temperature in a single experiment. In order to fully describe the phase diagram we also determined the phase boundaries between the solid phases and melt (these data also contribute to the determination of the melting curve to 70 GPa described by Lord et al. (2014)). Melting was accompanied in one experiment at 6 GPa at the NSLS by: (i) loss of Bragg reflections and appearance of diffuse scattering in diffraction patterns collected from the sample; (ii) visible variations in the absorption intensity of the sample due to flow of liquid NiSi; (iii) shortly thereafter a Re marker foil fell through the sample indicating that it had completely melted (see supplementary video in Lord et al., 2014).

Unit-cell parameters for the orthorhombic strain analysis of the distorted-CuTi structure (Section 3.4) were determined from diffraction patterns collected at DORIS by fitting Gaussian peaks to the 101, 002, 110, 102 and 012 reflections using a least-squares fitting procedure. Unique peak intensities and widths for each reflection were allowed to vary, along with the unit-cell lengths in the fit. A straight-line background correction was added

to the fit based on the X-ray intensity in the diffraction patterns 2.5σ from the centroid of the Gaussian fit. In the case of the diamond-anvil cell experiments at the ESRF (see below), unit-cell parameters were obtained by Le Bail fitting using the GSAS suite of programs (Larson and Von Dreele, 1994; Toby, 2001).

In addition to the *in situ* multi-anvil experiments described above we also report relevant results from three quenching experiments in the multi-anvil press at UCL and from two *in situ* diamond-anvil cell experiments at the ESRF, which are described in detail elsewhere (Wood et al., 2013; Lord et al., 2014), and a further three quenching multi-anvil and diamond-anvil experiments which were performed following the procedures described in those papers. The conditions, methods and identified phases for all experiments reported here are given in the Supplementary data.

3. Results

Representative diffraction patterns of NiSi samples in the MnP (*Pnma*), distorted-CuTi (*Pmmn*) and ε-FeSi ($P2_13$) stability fields, collected during one experiment at DORIS are presented in Fig. 2. The large reflections in the regions marked in grey in the figure come from the MgO pressure medium and Inconel furnace; at the 2θ of 3.22° that was used, a 500 μm wide X-ray beam has a diffracting volume which is ~15 mm long, of which only the central 1 mm contained the NiSi/NaCl sample. However, while diffraction from the pressure medium and Inconel furnace masks a substantial region of the diffraction pattern, Fig. 2 shows that there are sufficient unique reflections from the sample for phase identification. The ambient-pressure MnP phase persists metastably in the top diffraction pattern, collected at 12 GPa and room temperature during cold compression, but shows some strain-induced line broadening. Upon heating, the NiSi rapidly transforms to the distorted-CuTi phase and the transformation is complete by 753 K (middle trace). The clear splitting of the 1 0 2 and 0 1 2 reflections at 1.81 and 1.89 Å confirms that this phase is, indeed, the orthorhombically distorted structure previously seen in samples recovered from high pressure (Wood et al., 2013) and not the tetragonal γ-CuTi phase with space group *P*4/*nmm*. At higher temperatures, this distorted-CuTi phase transforms to the cubic ε-FeSi structure, but this transformation is sluggish and some peaks of the distorted-CuTi phase remain even after several hours in the ε-FeSi stability field. This is seen in the small reflection at 2.3 Å in the lower trace, collected at 16 GPa and 1218 K.

3.1. The phase diagram of NiSi to 19 GPa

Fig. 3 shows the phase diagram of NiSi determined by *in situ* multi-anvil experiments up to 19 GPa, along with the P-T conditions of previously reported experiments. Three solid phases were observed in these experiments: at pressures below 10–13 GPa, the MnP structure is the stable structure of NiSi, with the ε-FeSi structure becoming stable at high pressure and temperatures above ~1063 K and the distorted-CuTi structured phase (with space group *Pmmn*) stable at high pressure and temperatures below 1063 K. The invariant point between the three phases is located at 12.8 ± 0.2 GPa and 1100 ± 20 K.

The Clapeyron slope of the phase boundary between the MnP and distorted-CuTi phases is positive with $dP/dT = 3 \pm 0.75$ MPa/K. This extrapolates to a 0 K transition pressure of 9.5 ± 1 GPa, which is somewhat lower than predicted for this transition pressure by *ab initio* simulations (21 GPa; Wood et al., 2013). Similar discrepancies between predicted and observed transition pressures, however, are not uncommon for similar systems; see, for example, Dobson et al. (2002) and Vočadlo et al. (1999) for the ε-FeSi to CsCl transition in FeSi.

The ambient-pressure MnP-structured phase of NiSi transforms to the ε-FeSi structure at 12.8 ± 0.1 GPa and 1153 K. The Clapeyron slope of this transition was estimated from quenching experiments to be −10 ± 2 MPa/K. This results in a second invariant point, between the MnP-structured, ε-FeSi-structured and liquid phases at 9.5 ± 0.6 GPa and 1480 ± 70 K. This location is not well constrained in the multi-anvil press experiments as melt was only detected in one experiment, at low pressure, on the MnP-liquid boundary. However, the location of this invariant point determined from laser-heated diamond-anvil experiments (14 ± 4 GPa and 1590 ± 100 K; Lord et al., 2014) is consistent with this study.

3.2. The phase boundary between the ε-FeSi and the distorted-CuTi structure

The phase boundary between the ε-FeSi structure and the distorted-CuTi structure of NiSi occurs at 13 ± 0.1 GPa and

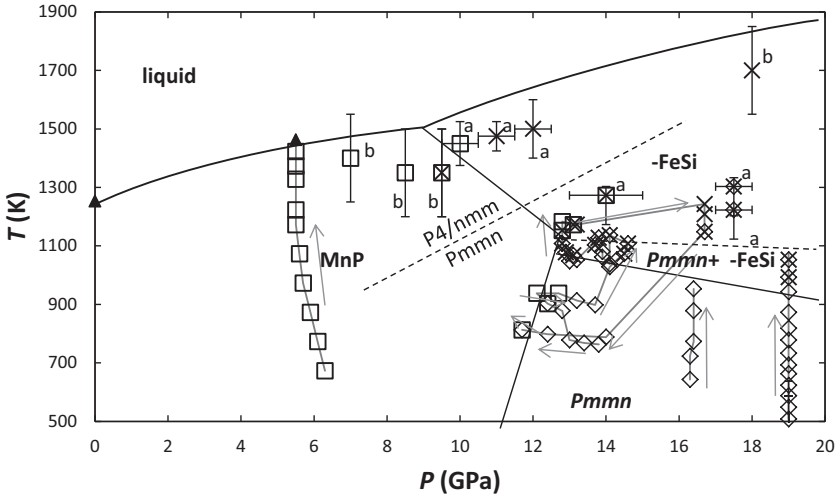

Fig. 3. The phase diagram of NiSi to 19 GPa. Arrows show the pressure-temperature paths of the *in situ* experiments. Data marked 'a' are from quenching multi-anvil experiments at UCL and those marked 'b' are from diamond-anvil cell experiments (Lord et al., 2012). The region of phase coexistence between the ε-FeSi and distorted-CuTi phases is delimited by the nearly horizontal dashed line. The diagonal dashed line marks the metastable phase boundary for the ferroelastic transition between the γ -CuTi (*P*4/*nmm*) structure and the distorted-CuTi (*Pmmn*) structure, calculated as described in Section 3.4. Symbols are as follows: MnP structure, open squares; distorted-CuTi structure, open diamonds; ε-FeSi structure, crosses; Molten FeSi, filled triangles.

1070 ± 10 K with a small negative Clapeyron slope. Unlike the other phase transitions reported here, a significant region of phase coexistence was observed at this boundary, as indicted in Fig. 3, with no discernible change in diffraction intensity with time if samples were held at constant P-T conditions for durations of up to 60 min. The *in situ* experiments were designed to rapidly determine the phase diagram across a wide region of P-T space and hence samples were not held at any one condition for more than 60 min; however, we have good reason to believe that for the bulk composition of the present experiments the region of phase coexistence is thermodynamically stable and not just a kinetic effect. A quenching experiment was performed at UCL, in which the sample was held at 17.5 GPa and 1223 K for 25 h (see Wood et al., 2013 for further details). X-ray diffraction of the sample, recovered to atmospheric pressure and room temperature, revealed a mixture of ε-FeSi and distorted-CuTi phases, while Electron Probe and SEM analysis (Fig. 4) determined the sample to be an intimate mixture of two phases with compositions of $Ni_{49.84}Si_{50.16}$ and $Ni_{53}Si_{47}$. The near-stoichiometry phase was the majority phase, comprising 86 ± 1% by volume of the sample, which agrees well with the phase proportion of distorted-CuTi phase derived from Rietveld refinement of the diffraction pattern of the sample (85 wt.%). While the phase proportion varied with the temperature of the experiment (a sample quenched from 1310 K contained only 40% distorted-CuTi phase, estimated from SEM images) the intimate mixture of the two phases demonstrates that the phase coexistence is not just due to thermal gradients in the cell. We suggest, rather, that the ε-FeSi phase of NiSi can accept an excess of Ni in its structure, changing the chemical system into a two-component system with a small finite field in *P-T* space of phase coexistence. Furthermore, once a portion of the sample is away from stoichiometry, the back-reaction to a single composition will be rate-limited by chemical diffusion, leading to the metastable persistence of both the distorted-CuTi and ε-FeSi phases across this boundary. Similar deviations from stoichiometry are well documented for other ε-FeSi structured metal silicides (e.g. Buschinger et al., 1997 for RuSi; Vočadlo et al., 1999 for FeSi).

3.3. Melting of NiSi

The melting curve of NiSi has been constrained to pressures just below the MnP-ε-FeSi-liquid invariant point by direct observation at 5.5 GPa as follows: first, at 1423 K recrystallization of the NiSi sample resulted in rapid and substantial changes in intensity in diffraction peaks in the sample. Second, on heating to 1463 K the radiographic images showed movement related to flow of the dense NiSi sample. Finally, on further heating a Re foil placed at the top of the sample settled through it confirming that it was completely molten: at this point the diffraction patterns showed no reflections from NiSi, but diffuse scattering was observed. We chose 1443 ± 20 K as the melting temperature since the recrystallization at 1423 K is a commonly observed pre-melting phenomenon while flow of the sample at 1463 K confirms that melt was present by this temperature. This is a congruent melting point since no new diffraction peaks appeared on loss of the MnP reflections and appearance of diffuse scattering. See supplementary video in Lord et al. (2014).

3.4. The orthorhombic distortion of the CuTi phase and the phase boundary of a possible Pmmn to P4/nmm transition

In the paper that reported the discovery of the distorted-CuTi phase of NiSi (space group *Pmmn*; Wood et al., 2013) the formation of this structure was described in terms of a ferroelastic distortion of a tetragonal, paraelastic phase with *P*4/*nmm* symmetry; in the Aizu (1969) classification, this ferroelastic, non-ferroelectric, transition is of species 4/*mmmFmmm*. In our earlier work (Wood et al., 2013), static (effectively 0 K) *ab initio* simulations using density functional theory were presented which showed that the degree of orthorhombic distortion increased with pressure and continued to decrease when simulations were performed at volumes corresponding to negative pressures. It was suggested, therefore, that the *P*4/*nmm* tetragonal structure might form the stable phase of NiSi at elevated temperature.

In the present study, we have never directly observed the *Pmmn* to *P*4/*nmm* transition but we have been able to infer the locus of

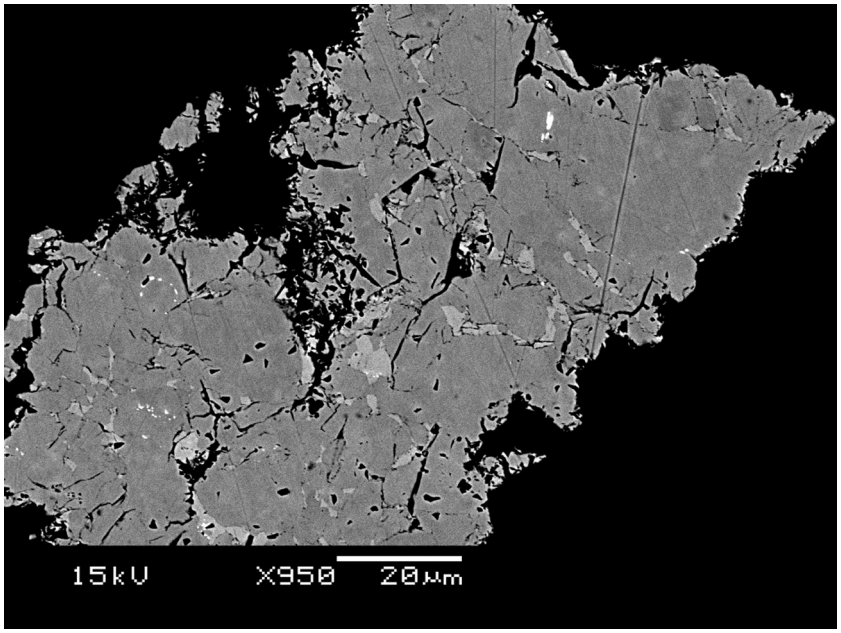

Fig. 4. Backscattered electron image of a recovered sample equilibrated at 17.5 GPa and 1223 K for 25 h and containing both the ε-FeSi (brighter) and distorted-CuTi (darker) structures.

this phase boundary in P/T space from analysis of the degree of orthorhombic distortion observed in our experiments. This orthorhombic distortion is best characterised by the spontaneous strain, ε^S, defined by Aizu (1970), which can be taken as the order parameter for the phase transition. In principle, the spontaneous strain should be calculated from $\varepsilon^S = (1/\sqrt{2})\,[(a_O - b_O)/a_T]$, where a_T is the lattice parameter of the high-symmetry, tetragonal phase extrapolated into the orthorhombic phase field, since in this way the thermal expansion and distortion contributions to the changes in the lattice parameters can be separated (see e.g. David and Wood, 1983). In the present case, however, this procedure could not be used as the tetragonal phase was never seen and the spontaneous strain was, therefore, calculated from the orthorhombic cell parameters, a_O and b_O, using the relation $\varepsilon^S = (1/\sqrt{2})\,[(a_O - b_O)/\sqrt{(a_O b_O)}]$. Since the term a_T appears only in the denominator of the expression for ε^S, the alternative approximation, that $a_T = (a_O + b_O)/2$, leads to almost identical values.

Fig. 5a shows the values of ε^S observed in the Pmmn phase as a function of pressure and temperature in the present experiments; it is clear that ε^S increases with P and decreases with T. The curves shown in the Figure give the temperature dependence of ε^S at selected pressures calculated on the basis that: (i) the phase transition is of second order (i.e. is continuous, which is allowable as *Pmmn* is a subgroup of *P*4/*nmm*), (ii) the temperature-dependence of ε^S follows a mean-field like behaviour, (iii) the transition temperature, T_C, varies linearly with P, and (iv) the saturation value of ε^S (i.e. its value at $T = 0$ K) varies linearly with P. None of these assumptions is necessarily correct (see e.g. Lines and Glass, 1977); indeed, our VASP simulations (Fig. 5b) indicate a pronounced non-linearity in the saturation value of ε^S at higher pressures, but we believe that they are adequate for the purpose of estimating the position of the phase boundary. It is clear from the data points in Fig. 5a that the observations lie outside the temperature range in which the mean-field approximation that ε^S is

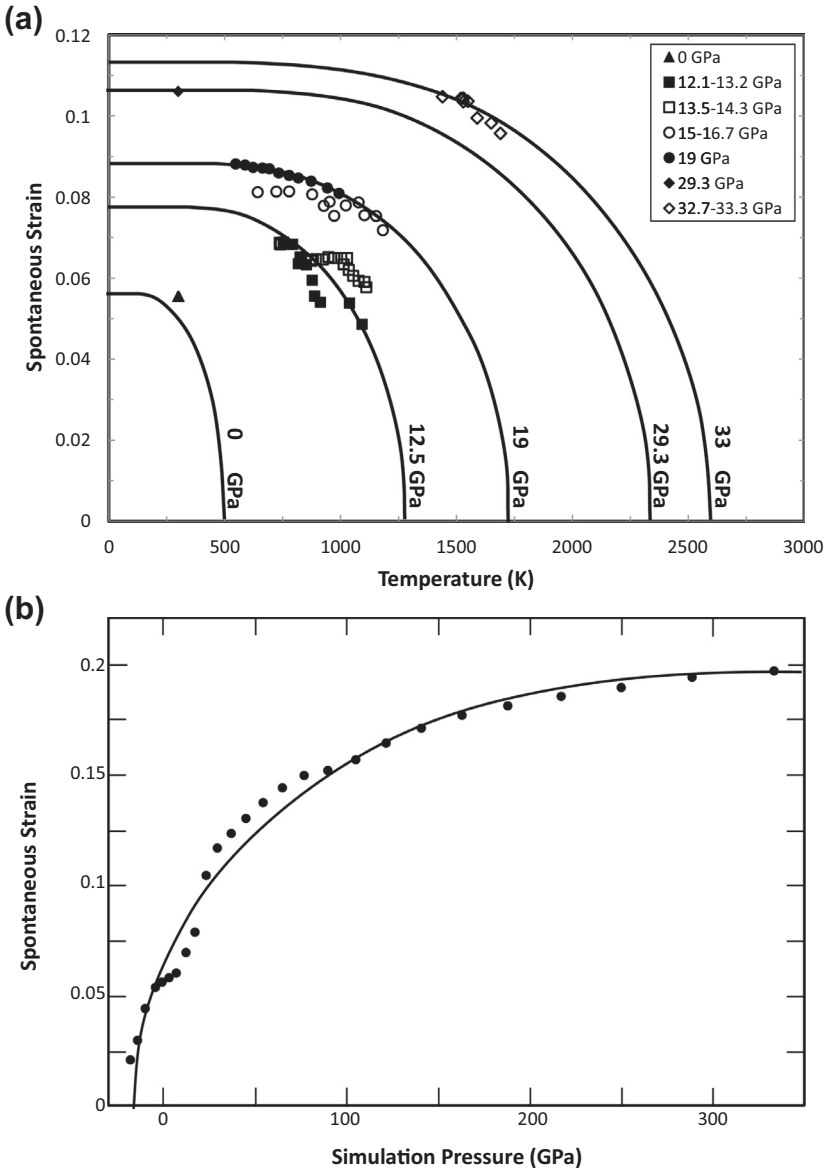

Fig. 5. (a) Spontaneous strain, ε^S, versus temperature for the distorted-CuTi (*Pmmn*) phase of NiSi, with respect to the tetragonal, γ-CuTi (*P*4/*nmm*) paraelastic structure. Data points were determined as described in Section 2 and the 0 GPa datum is from Wood et al. (2013). The data at 19 GPa can be considered isobaric; for convenience in display, the remaining data are labelled according to the pressure range in which they fell (note, however, that the actual pressure values of each point were used in the data analysis). The lines correspond to a mean-field approximation for the temperature and pressure dependence of ε^S (see Section 3.4 for details), drawn for selected isobars at 0, 12.5, 19, 29.3 and 33 GPa. (b) Spontaneous strain, ε^S, from static (0 K) VASP simulations (Wood et al., 2013) versus pressure for the *Pmmn* phase of NiSi, with respect to the tetragonal, γ-CuTi (*P*4/*nmm*) paraelastic structure. The line corresponds to a mean-field approximation for the pressure dependence of ε^S (see Section 3.4 for details).

proportional to $\sqrt{(T - T_C)}$ would be valid; instead a fully self-consistent mean-field formulation was needed, capable of describing the behaviour of ε^S over the complete temperature range. Initially, a model based on the quasi-harmonic approach used by David and Wood (1983) was employed, but a much better representation of ε^S could be obtained by using the approach previously adopted by Wood et al. (2004) to describe the effects of magnetostriction on the cell volume of Fe_3C, which is based on numerical solutions of the intersection of a Brillouin function ($B_{1/2}(y)$ in this case) with a line whose slope is proportional to temperature (for further details see Wood et al., 2004). With these assumptions we were able to describe the evolution of ε^S as a function of P and T in terms of four adjustable parameters: (a) T_C at $P = 0$; (b) $\partial T_C/\partial P$; (c) $\varepsilon^S(P,T)$ at $P = 0$, $T = 0$; (d) $\partial\varepsilon^S/\partial P$ at $T = 0$. We found that the data were not adequate to allow all four parameters to be fitted simultaneously by non-linear least squares, so a two stage process was adopted. Firstly, we determined the parameters (c) and (d) above by fitting the data collected at 19 GPa, (indicated by the filled circles in Fig. 5a) so as to obtain the saturation value of ε^S at this pressure (we chose these data as we considered them to be the most reliable). We then used this saturation value of ε^S, together with the spontaneous strain at 29.3 GPa and 300 K (indicated by a filled diamond in Fig. 5a) to determine the rate of change of the saturation value of ε^S with respect to pressure. This gave the relation $\varepsilon^S(T = 0) = 0.0553(1) + 0.00174P$, where P is in units of GPa (no estimated uncertainty is quoted for the parameter (d) as it was obtained from values at only two pressures). The remaining parameters, (a) and (b) above, were then determined by fitting simultaneously to the complete data set, from which we obtained the relation $T_C = 502(48) + 64(3)P$, where T_C is in K and P in GPa. Bearing in mind that many of the data shown in Fig. 5a show considerable scatter, we consider our representation of the behaviour of ε^S to be quite satisfactory. When T_C is plotted as a function of P on the NiSi phase diagram (Fig. 3), it becomes apparent that the tetragonal, $P4/nmm$, phase of NiSi will never be thermodynamically stable. There is, however, the possibility that it might be observed, metastably, by heating the $Pmmn$ phase at atmospheric pressure since, at $P = 0$, $T_C = 502$ K, which might be a sufficiently low temperature for the phase transition to be observed before the NiSi reverts to the MnP structure.

The behaviour of ε^S as a function of pressure as determined in our *ab initio* simulations at $T = 0$ K (Wood et al., 2013) is shown in Fig. 5b. The line shown in the figure is again based on the mean-field theory described above, with two parameters (the transition pressure and the saturation value of ε^S) fitted by non-linear least squares to the data. The transition pressure at $T = 0$ K was thereby determined from the VASP simulations to be $-16(1)$ GPa, in satisfactory agreement with the extrapolated value from our experimental results (above), from which a transition pressure of $-8(1)$ GPa is expected at 0 K.

3.5. Extension of the phase diagram to higher pressures

In addition to the multi-anvil experiments, we also report here the results from two exploratory laser-heated diamond anvil cell experiments with simultaneous synchrotron X-ray diffraction at 29–35 and 60–65 GPa. Experimental details for these experiments are described in detail in Lord et al. (2014), which focusses on the melting curve of NiSi to 70 GPa. The phase diagram of NiSi is extended to 65 GPa in Fig. 6a. In both experiments reported here, fresh samples of MnP-structured starting material were compressed at room temperature to the pressure of interest and then heated by double-sided laser heating.

At 33 ± 1 GPa, MnP-structured NiSi transformed to a mixture of the distorted-CuTi and ε-FeSi structured phases on initial heating to 1440 K. The distorted-CuTi phase persisted in diffraction patterns to 1690 K, after which only ε-FeSi structured NiSi was observed until 34.4 ± 1.3 GPa and 2165 K. Above this temperature X-ray diffraction patterns showed reflections from a new phase, consistent with the CsCl structure, plus diffuse scattering indicative of the presence of melt. The CsCl structure was determined to be the phase stable at the highest pressures of the static *ab initio* simulations of Vočadlo et al. (2012) and the laser-heated diamond anvil cell experiments of Lord et al. (2012). The simultaneous appearance of the CsCl phase with liquid suggests that the ε-FeSi + CsCl + liquid invariant point occurs slightly below the pressure and temperature of this experiment (this is identical to the invariant point in Lord et al. 2014, which is quoted as 28.5 ± 1.5 GPa and 2165 ± 60 K, without the contribution of thermal pressure for comparison with off-line experiments). There is also, however, a large region over which the distorted-CuTi and ε-FeSi phases coexist in this experiment (1440–1660 K), with the distorted-CuTi phase persisting to higher temperatures than predicted from the multi-anvil experiments. While this might be a real property of the material it might also be explained either by thermal gradients in the cell if the X-ray spot was not perfectly aligned with the laser heated spot, or by the region sampled in this experiment unfortunately containing some of the δ-Ni_2Si material which was seen on the grain boundaries of the starting material. The size of the beam used in these experiments was only 3 × 3 μm; with such a small diffraction volume, this grain-boundary impurity might be sufficient to enhance any effects of non-stoichiometry on the stability of these phases and, indeed, to reduce the melting temperature somewhat.

At 60 GPa the first phase assemblage to be produced on very gentle laser heating was a mixture of distorted-CuTi and ε-FeSi structured NiSi. At this point, the sample was too cool for spectroradiometric temperature measurement, implying that the temperature was below ~1200 K. While this does not place any further constraints on the Clapeyron slope of the phase boundary between the distorted-CuTi and ε-FeSi structures it is consistent with the phase boundary extrapolated from the multi-anvil experiments. On further heating, to 1360 K, reflections from the distorted-CuTi phase disappear and pure ε-FeSi is observed. This persists to 1680 K and at 1750 K the CsCl phase becomes stable. Melting is observed at 2480 K, by the appearance of diffuse scattering in the diffraction pattern. The phase boundary between the ε-FeSi and CsCl structures in NiSi determined from these two experiments has a Clapeyron slope of −67 MPa/K, consistent with constraints from Lord et al. (2012) who bracketed the transition at 46 ± 3 GPa and 1900 ± 150 K (points labelled 'a' in Fig. 6a). Extrapolation of this boundary to 0 K leads to a metastable ε-FeSi to CsCl transition pressure of 173 ± 40 GPa, which is in good agreement with the static *ab initio* simulations (171 GPa; Vočadlo et al., 2012). The small pressure dependence of the distorted-CuTi to ε-FeSi phase boundary implies the possibility of a second subsolidus invariant point between these phases and the CsCl phase of NiSi. This is very approximately located at 162 GPa and 120 K by extrapolation from the present data, suggesting that the ε-FeSi phase is never stable at 0 K, in agreement with the simulations results. Finally, we note that the Clapeyron slope of the ε-FeSi to CsCl boundary is similar to that in FeSi determined by Lord et al. (2010), but very different from the boundary determined recently by Fischer et al. (2013) where ε-FeSi and CsCl structured FeSi coexist from 10 to 40 GPa and then react to form pure CsCl-FeSi. An even more recent study indicates a mixed-phase field from 25 to 30 GPa (Geballe and Jeanloz, 2012). As with the distorted-CuTi to ε-FeSi transition studied here, the field of phase coexistence between the ε-FeSi and CsCl structured FeSi structures might be enhanced by kinetic effects in both studies but this will only be clarified with further work.

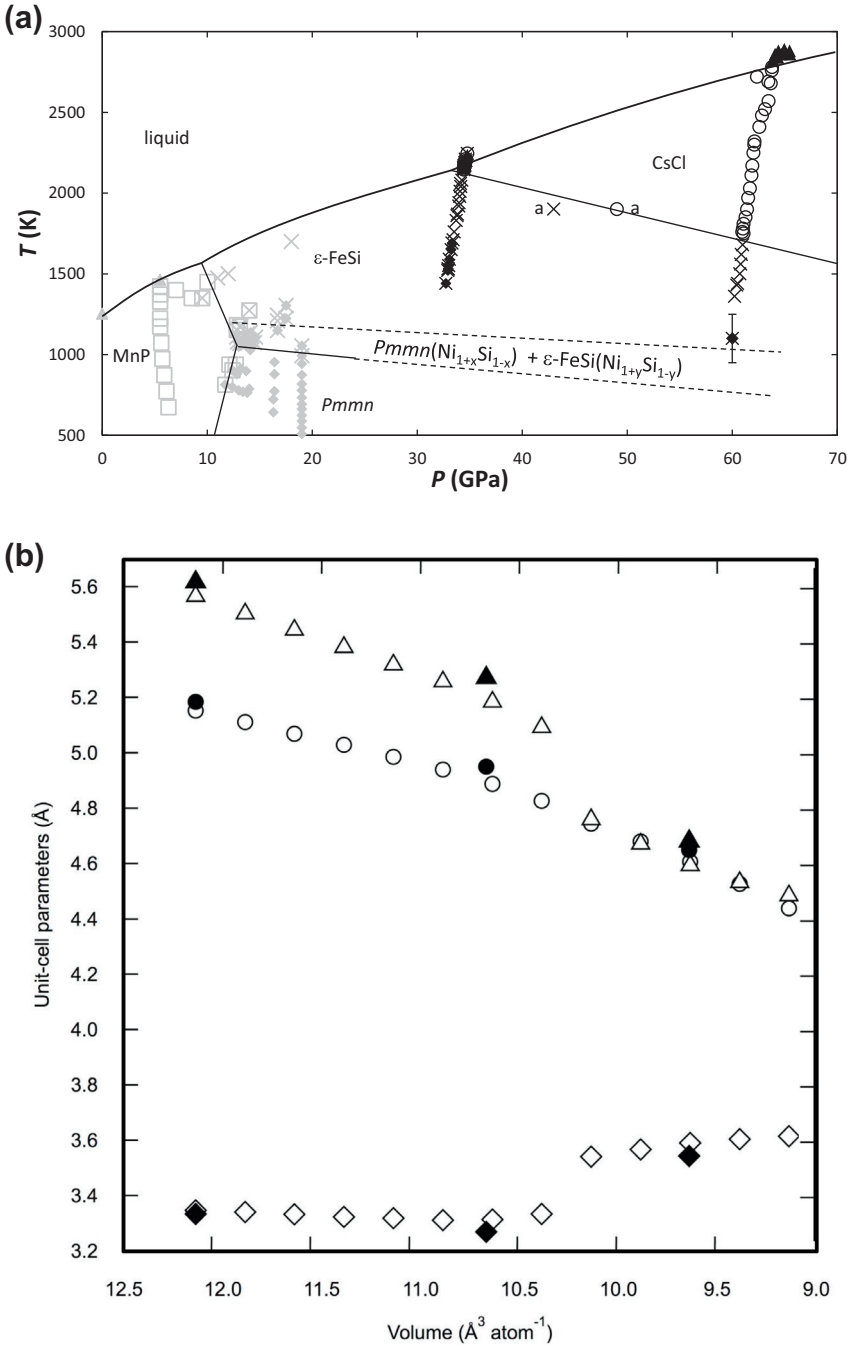

Fig. 6. Preliminary sub-solidus phase relations in NiSi to 65 GPa based on laser-heated diamond-anvil-cell experiments. (a) Extension of the pressure-temperature phase diagram to 65 GPa. Symbols are the same as in Fig. 3 with the addition that circles represent the CsCl structure. Grey symbols are the data from Fig. 3 and black symbols are from the laser-heated diamond anvil cell experiments of Lord et al. (2014). The points labelled 'a' are from Lord et al. (2012). (b) Unit cell parameters plotted against cell volume for compression of MnP-structured NiSi to 60 GPa, showing a metastable transition to the *Pmna*-II structure at ~40 GPa (V ~ 10.5 Å^3 atom^{-1}). Solid symbols are experimental values from this study and open symbols are static (0 K) *ab initio* simulation values from Vočadlo et al. (2012), corrected to the experimental volumes (see Section 3.6). Circles = *a-axis*, diamonds = *b-axis*, triangles = *c-axis*.

3.6. A new metastable phase of NiSi at 60 GPa and 300 K

In addition to these stable phases described above, the diamond-anvil cell study also revealed that on compression to 60 GPa at room temperature the MnP-structured starting material had transformed to a new structure of NiSi (also with space group *Pnma*) that had been discovered and labelled *Pnma*-II in the static *ab initio* simulations of Vočadlo et al. (2012). The change in structure was identified from the changes in the unit-cell parameters in samples compressed to 35 GPa and 60 GPa at room temperature, prior to laser heating. Unfortunately, full Reitveld refinement was not possible since this was a small component of the total diffracting volume with quite variable intensities (see for instance Lord et al., 2014 Fig. 7). These reflections were therefore fitted using the LeBail method and hence assignment of this metastable phase to the *Pnma*-II structure is based on (1) the systematic presence of only strong reflections of the *Pnma*-II structure in the diffraction patterns and (2) the agreement of unit-cell parameter evolution

in the experiments with the simulations of Vočadlo et al. (2012). The experimental unit-cell parameters are plotted in Fig. 6b as a function of unit cell volume, together with the values from the simulations (Vočadlo et al., 2012) corrected approximately to the experimental volumes by subtracting a constant volume offset on the X-axis of the plot of 0.1392 Å^3/atom from each simulation point. The agreement between the two studies is excellent. In the static (0 K) simulations the ambient pressure MnP-structured NiSi spontaneously transformed to the *Pnma*-II structure at ~42 GPa, consistent with the experiments which bracketed the transition between 35 GPa and 60 GPa at 300 K. The simulations then predicted a further transformation of the *Pnma*-II phase at a pressure of ~63 GPa to a structure that was labelled *Pnma*-III by Vočadlo et al. (2012). Although the MnP, *Pnma*-II and *Pnma*-III structures are isosymmetric, their axial ratios and atomic coordinates are quite distinct and there are major differences in the primary coordination of the atoms. As described in detail by (Vočadlo et al., 2012) the six fold primary coordination of each atom in the MnP structure increases to 11-fold in the *Pnma*-II phase, with each atom surrounded by seven atoms of the other species and four atoms of the same species. In the *Pnma*-III phase, which we have not yet observed experimentally but which may well form at room temperature at a pressure above 60 GPa, the primary coordination of the atoms is increased to 12; in the *Pnma*-III structure both atoms have almost perfect 12-fold anticuboctahedral coordination by eight atoms of the other kind and four atoms of the same kind.

However, although the *Pnma*-II phase of NiSi clearly exists, since it has now been observed experimentally as well as in computer simulations, our results show that it is never the thermodynamically most stable phase of NiSi at any pressure or temperature. At 0 K, computer simulations show that the distorted-CuTi phase has a lower free energy than *Pnma*-II at all pressures (Wood et al., 2013), whereas in the present study we have determined that although *Pnma*-II is a lower energy structure than the MnP structure at 60 GPa, it transformed to the distorted-CuTi structure on heating. Thus, the *Pmmn* structure is more stable than *Pnma*-II at both 0 K (from the simulations) and high temperature (from the present experiments), implying that *Pnma*-II must be a metastable phase of NiSi.

4. Discussion and conclusions

4.1. Comparison with previous work

The phase diagram of NiSi determined in the present simultaneous high-*P*/*T* study is in good agreement with the results obtained previously by quenching experiments (Lord et al., 2012; Wood et al., 2013). As indicated in Fig. 3 and Fig. 6a, four thermodynamically stable phases of NiSi have now been observed in our experiments, namely: the MnP-structured ambient-pressure phase, an orthorhombically distorted CuTi structure with space group *Pmmn*, an ε-FeSi structured form and a form with the CsCl structure. These findings are also in very good accord with the revised results obtained from static *ab initio* simulations (Wood et al., 2013), in which the MnP, distorted-CuTi and CsCl structures were determined to be the stable phases at 0 K. The fact that the ε-FeSi structured form of NiSi was never the thermodynamically most stable phase in the simulations is exactly as would be expected from our experimental results as the ε-FeSi phase field (Fig. 6a) is bounded by the MnP, distorted-CuTi and CsCl structured phases (and the melt) and so does not extend to 0 K at any pressure. Were it possible to perform experiments at 0 K, Fig 6a shows that the sequence of stable phases of NiSi would be exactly as expected from the simulations. The free energy difference between the distorted-CuTi and ε-FeSi structures, however, is only about 30 meV atom^{-1} (Wood et al., 2013), which may be easily overcome by thermal energy (30 meV being equivalent to ~350 K) and so it is not at all surprising to find that ε-FeSi structured NiSi becomes more stable than the distorted-CuTi structure above about 1100 K. The study of Gavryushkin et al. (2015) predicted that the CsCl-structured phase of NiSi should have a significant tetragonal distortion (with c/a ~ 0.8) at all pressures below 522 GPa, however the LHDAC experiments reported here and elsewhere (Lord et al., 2014) show no evidence for this large distortion under any P-T conditions where CsCl-NiSi was observed.

The experiments presented here have also confirmed several of the suggestions made previously (Vočadlo et al., 2012; Lord et al., 2012; Wood et al., 2013) with regard to possible metastable phases of NiSi. Firstly, it is now clear that compression of the MnP structured ambient pressure phase of NiSi at room temperature does, indeed, produce a transition, at a pressure between 35 and 60 GPa, to the phase labelled *Pnma*-II in Vočadlo et al. (2012) and predicted therein to form at ~42 GPa. By extension, it is therefore reasonable to suppose that experiments at room temperature and still higher pressure will result in a further transition to the phase labelled *Pnma*-III in the computer simulation study. Secondly, we have now been able to predict with reasonable confidence the phase boundary for the ferroelastic distorted-CuTi (*Pmmn*) – γ-CuTi (*P*4/*nmm*) transition discussed by Wood et al. (2013). Our results (see Fig. 5a and Fig. 3) show that this transition will occur within the stability fields of the MnP and ε-FeSi structures of NiSi and thus the tetragonal γ-CuTi phase of NiSi will never be thermodynamically stable. Since the distorted-CuTi structure of NiSi may be recovered to ambient conditions, it is, however, possible that the ferroelastic transition might be observed metastably at atmospheric pressure, as the expected transition temperature (~500 K) may then be sufficiently low that conversion to the stable MnP structure is kinetically inhibited. Finally, the very close correspondence between the results of the static computer simulations and the experiments suggests that it may indeed be possible to produce, metastably, at least some of the other forms of NiSi that were predicted to have free energies only a few tens of meV atom^{-1} greater than those of the thermodynamically most stable structures (Vočadlo et al., 2012; Wood et al., 2013). Some indication that this might be so was observed in the earlier laser-heated diamond-anvil cell study of Lord et al. (2012), in which a few low-intensity X-ray reflections were seen which might have been consistent with several of the structures predicted in the *ab initio* study and which were interpreted as possible quench phases or phases which had grown at the low-temperature edges of the laser-heated spot. This highlights one advantage of systematic structure searches, as implemented by Vočadlo et al. (2012) over structure prediction software (eg Gavryushkin et al., 2015) in that the prediction software only predicted stable structures and not the metastable structures which we have produced in the laboratory.

4.2. Implications for planetary interiors

The phase diagram of NiSi is significantly different from that of FeSi at low pressures and temperatures, with two additional stable phases and several metastable phases not seen in the FeSi system. At pressures and temperatures above 13 GPa and 1000 K, however, the two compositions show remarkably similar phase diagrams, though with some pressure shift between them. This suggests that there will be solid-solution between NiSi and FeSi at high pressure and that incorporation of small amounts of nickel will not significantly affect the behaviour of the iron-silicon system in the cores of Earth-size and larger planets (see Lord et al. 2014 for discussion). In smaller planets, the stability of the MnP structure of NiSi to 13 GPa (by which time in the FeSi system the CsCl structure is on

the liquidus) and the difference in pressure between the transitions from the ε-FeSi to CsCl structures (~24 GPa at 1950 K in FeSi from Dobson et al. (2000) and 46 GPa at 1900 K in NiSi, Lord et al., 2012) will result in eutectic behaviour at pressures below ~30 GPa. Nickel might therefore help to depress the liquidus in smaller planetary bodies such as Mercury whose core pressures fall in this range (7–40 GPa) and which has a liquid core thought to be rich in silicon (Malavergne et al., 2010). This might reduce the need for a very high sulphur content in the core of Mercury (e.g. Harder, 2001; Rivoldini et al., 2009) which has been invoked to reduce the solidus temperature but which has little cosmochemical justification (e.g. Goettel, 1988). We note here that the Si contents of planetary cores will be significantly below 50 mol.% and hence studies of the more Si-poor Fe-Ni-Si alloys are required; however the present study shows that the Ni-Si system is significantly different from the Fe-Si system at the pressures of the smaller planets and satellites and hence significant eutectic depression should be expected in this ternary.

4.3. Implications for thin-film semiconductor technology

Although our primary motivation for the investigation of NiSi comes from its role in Earth and planetary sciences, NiSi is also an important material for complementary metal-oxide semiconductor (CMOS) technology as very thin films of NiSi may be used to form the contacts on silicon semiconductor substrates (see e.g. Lavoie et al., 2006, 2007; Li et al., 2009). It now seems to be generally accepted that when thin films of NiSi are grown on either Si (1 0 0) or Si(1 1 1) substrates by annealing a deposited layer of either Ni or Ni/Si, the resulting film (when annealing is complete) consists of NiSi with the room-pressure MnP structure (e.g. d'Heurle et al., 1984). However, during the annealing processes, transient nickel silicide phases form, the nature of which is still somewhat uncertain (d'Heurle et al., 1984; De Keyser et al., 2008; Van Bockstael et al., 2009; Hoummada et al., 2010; Lu et al., 2013). The high-P/T phase diagram of NiSi may well have some relevance for this work, since it is well known that thin films of FeSi with the high-pressure CsCl-type structure can form on Si (1 1 1) substrates (von Känel et al., 1992, 1994; Kafader et al., 1993), despite the fact that, at the temperatures at which these films are grown (300–800 K), pressures well in excess of 20 GPa are required to produce this phase in bulk samples of FeSi (Dobson et al., 2002; Lord et al., 2010). Several possible orientations of the high-pressure nickel silicides could be conceived which have reasonable strains; for example, an (0 1 1) surface of the *Pmmn* phase of NiSi fits the Si(1 0 0) unit cell metric with 4 vol% strain, with Ni atoms coincident with the Si (0, 0, 0) atomic coordinate and Si atoms coincident with the Si (0, ½, ½) coordinate and further Ni and Si atoms at (0, ½, 0) and (0, 0, ½) respectively.

Acknowledgements

This work was supported by the Natural Environment Research Council (NERC) through grants to LV (NE/H003975/1), DPD (NE/J009520/1) at UCL, MJW at Bristol (NE/H003541/1) and a postdoctoral research fellowship awarded to OTL at Bristol (NE/J018945/1). SAH was also supported by a NERC fellowship (NE/H016309/1) and AMW was supported by ERC grant 240473. RCUK provided Ph.D. studentships for EW (STFC) and JS (NERC). Use of the National Synchrotron Light Source, Brookhaven National Laboratory, was supported by the U.S. Department of Energy, Office of Science, Office of Basic Energy Sciences, under contract no. DE-AC02-98CH10886. Use of the X17B2 beamline was supported by COMPRES, the Consortium for Materials Properties Research in Earth Sciences under NSF Cooperative Agreement EAR 10-43050. Use of MAX200x was provided via DESY user access. Finally, we wish to thank Dr Devashibhai Adroja and Dr Kevin Knight (ISIS Facility, Rutherford Appleton Laboratory, U.K.) for assistance with sample preparation.

Appendix A. Supplementary data

Supplementary data associated with this article can be found, in the online version, at http://dx.doi.org/10.1016/j.pepi.2016.10.005.

References

Aizu, K., 1969. Possible species of "ferroelastic" crystals and of simultaneously ferroelectric and ferroelastic crystals. J. Phys. Soc. Jpn. 27, 387–396.
Aizu, K., 1970. Determination of the state parameters and formulation of spontaneous strain for ferroelastics. J. Phys. Soc. Jpn. 28, 706–716.
Antonangeli, D., Siebert, J., Badro, J., Farber, D.L., Fiquet, G., Morard, G., Ryerson, F.J., 2010. Composition of the Earth's inner core from high-pressure sound velocity measurements in Fe–Ni–Si alloys. Earth Planet. Sci. Lett. 295, 292–296Birch, F., . Elasticity and composition of the Earth's interior. J. Geophys. Res. 57, 227–286.
Birch, F., 1964. Density and composition of mantle and core. J. Geophys. Res. 69, 4377–4388.
Buschinger, B., Geibel, C., Diehl, J., Guth, W., Weiden, M., Wildbrett, A., Horn, S., Steglich, F., 1997. Preparation and low temperature properties of FeSi-type RuSi. J. Alloy. Compd. 256, 57–60.
Caracas, R., Wentzcovitch, R., 2004. Equation of state and elasticity of FeSi. Geophys. Res. Lett. 31, 20601–20604.
Chabot, N.L., Wollack, E.A., Klima, R.L., Minitti, M.E., 2014. Experimental constraints on Mercury's core composition, 390, 199–208, doi: 10.1016/j.epsl.2014.01.004.
David, W.I.F., Wood, I.G., 1983. Ferroelastic phase transition in $BiVO_4$: V. Temperature dependence of Bi^{3+} displacement and spontaneous strains. J. Phys. C: Solid State Phys. 16, 5127–5148.
Decker, D.L., 1971. High-pressure equation of state for NaCl, KCl, and CsCl. J. Appl. Phys. 42 (8), 3239–3244. http://dx.doi.org/10.1063/1.1660714.
Deng, L.W., Fei, Y.W., Liu, X., Gong, Z.Z., Shahar, A., 2013. Effect of carbon, sulfur and silicon on iron melting at high pressure: implications for composition and evolution of the planetary terrestrial cores. Geochim. Cosmochim. Acta, 220–233. http://dx.doi.org/10.1016/j.gca.2013.01.023.
De Keyser, K., Van Bockstael, C., Detavernier, C., Van Meirhaeghe, R.L., Jordan-Sweet, J., Lavoie, C., 2008. Epitaxial formation of a metastable hexagonal nickel-silicide. Electrochem. Solid State Lett. 11, H266–H268.
Dobson, D.P., Crichton, W.A., Vočadlo, L., Jones, A.P., Wang, Y., Uchida, T., Rivers, M., Sutton, S., Brodholt, J.P., 2000. In situ measurement of viscosity of liquids in the Fe-FeS system at high pressures and temperatures. Am. Mineral. 85, 1843–1847.
Dobson, D.P., Vočadlo, L., Wood, I., 2002. A new high-pressure phase of FeSi. Am. Mineral. 87, 784–787.
Dobson, D.P., Crichton, W.A., Bouvier, P., Vočadlo, L., Wood, I.G., 2003. The equation of state of CsCl-structured FeSi to 40 GPa; implications for silicon in the Earth's core. Geophys. Res. Lett. 30 (1014). http://dx.doi.org/10.129/2002GL016228.
Dobson, D.P., Hunt, S.A., McCormack, R., Lord, O.T., Weidner, D.J., Li, L., Walker, A.M., 2010. Thermal diffusivity of MORB to 15 GPa: implications for triggering of deep seismicity. High Press. Res. 30, 406–414. http://dx.doi.org/10.1080/08957959.2010.516827.
Dubrovinsky, L., Dubrovinskaia, N., Langenhorst, F., Dobson, D., Rubie, D., Geßmann, C., Abrikosov, I., Johansson, G., Baykov, V.I., Vitos, L., Le Bihan, T., Crichton, W.A., 2003. Iron-silica interaction at extreme conditions and the nature of the electrically conducting layer at the base of Earth's mantle. Nature 422, 58–61.
Fischer, R.A., Campbell, A.J., Reaman, D.M., Miller, N.A., Heinz, D.L., Dera, P., Prakapenka, V.B., 2013. Phase relations in the Fe–FeSi system at high pressures and temperatures. Earth Planet. Sci. Lett. 373, 54–64.
Gavryushkin, P.N., Popov, Z.I., Litasov, K.D., Gavryushkin, A., 2015. Unbiased crystal structure prediction of NiSi under high pressure. J. Appl. Crystallogr. 48, 906–908. http://dx.doi.org/10.1107/S1600576715005488.
Geballe, Z.M., Jeanloz, R., 2012. Origin of temperature plateaus in laser-heated diamond anvil cell experiments. J. Appl. Phys. 111 (12), 123518. http://dx.doi.org/10.1063/1.4729905.
Goettel, K.A., 1988. Present bounds on the bulk composition of Mercury: implications for planetary formation processes. In: Vilas, F., Chapman, C.R., Matthews, M.S. (Eds.), Mercury. Univ. of Arizona Press, Tucson, pp. 613–621.
Harder, H., 2001. Sulfur in mercury's core? Icarus 151, 118–122.
d'Heurle, F., Petersson, C.S., Baglin, J.E.E., La Placa, S.J., Wong, C.Y., 1984. Formation of thin films of NiSi: metastable structure, diffusion mechanisms in intermetallic compounds. J. Appl. Phys. 55, 4208–4218.
Hoummada, K., Blum, D., Mangelinck, D., Portavoce, A., 2010. Composition measurement of the Ni-silicide transient phase by atom probe tomography. Appl. Phys. Lett. 96, 261904.
Kafader, U., Tuilier, M.H., Pirri, C., Wetzel, P., Gewinner, G., Bolmont, D., Heckmann, O., Chandesris, D., Magnan, H., 1993. Formation of epitaxial CsCl-type iron silicide on Si(1 1 1). Europhys. Lett. 22, 529–535.
von Känel, H., Mäder, K.A., Müller, E., Onda, N., Sirringhaus, H., 1992. Structural and electronic properties of metastable epitaxial $FeSi_{1+x}$ films on Si(1 1 1). Phys. Rev. B 45, 13807–13810.

von Känel, H., Mendik, M., Mäder, K.A., Onda, N., Goncalves-Conto, S., Schwarz, C., Malegori, G., Miglio, L., Marabelli, F., 1994. Elastic and vibrational properties of pseudomorphic FeSi films. Phys. Rev. B 50, 3570–3576.

Kantor, A.P., Kantor, I.Y., Kurnosov, A.V., Kuznetsov, A.Y., Dubrovinskaia, N.A., Krisch, M., Bossak, A.A., Dmitriev, V.P., Urusov, V.S., Dubrovinsky, L.S., 2007. Sound wave velocities of fcc Fe–Ni alloy at high pressure and temperature by mean of inelastic X-ray scattering. Phys. Earth Planet. Inter. 164, 83–89.

Kuwayama, Y., Hirose, K., Sata, N., Ohishi, Y., 2008. Phase relations of Fe and Fe–Ni alloys up to 300 GPa: implications for composition and structure of the Earth's inner core. Earth Planet. Sci. Lett. 273, 379–385.

Larson A.C., Von Dreele R.B., 1994. General Structure Analysis System (GSAS). Los Alamos National Laboratory Report LAUR 86-748.

Lavoie, C., Detavernier, C., Cabral, C., d'Heurle, F.M., Kellock, A.J., Jordan-Sweet, J., Harper, J.M.E., 2006. Effects of additive elements on the phase formation and morphological stability of nickel monosilicide films. Microelectron. Eng. 83, 2042–2054.

Lavoie, C., d'Heurle, F.M., Zhang, S.-L., 2007. In: Nishi, Y., Doering, R. (Eds.), Chapter 10 in Handbook of Semiconductor Manufacturing Technology. 2nd ed. CRC Press, Boca Raton, FL.

Li, B., Luo, Z., Shi, L., Zhou, J., Rabenburg, L., Ho, P.S., Allen, R.A., Cresswell, M.W., 2009. Controlled formation and resistivity scaling of nickel silicide nanolines. Nanotechnology 20, 085304.

Lines, M.E., Glass, A.M., 1977. Principles and Applications of Ferroelectrics and Related Materials. Clarendon Press, Oxford.

Lord, O.T., Walter, M.J., Clark, S., Armstrong, L., Kleppe, A., Dobson, D.P., 2010. The FeSi phase diagram to 150 GPa. J. Geophys. Res. 115, B06208.

Lord, O.T., Vočadlo, L., Wood, I.G., Dobson, D.P., Clark, S.M., Walter, M.J., 2012. High-pressure phase transitions and equations of state in NiSi II: experimental results. J. Appl. Crystallogr. 45, 726–737. http://dx.doi.org/10.1107/S0021889812016809.

Lord, O.T., Wann, E., Hunt, S.A., Walker, A.M., Santangeli, J., Walter, M.J., Dobson, D. P., Wood, I.G., Vočadlo, L., Morard, G., Mezouar, M., 2014. The NiSi melting curve to 70 GPa. Phys. Earth Planet. Inter. 233, 13–23.

Lord, O.T., Thomson, A.R., Wann, E.T.H., Wood, I.G., Dobson, D.P., Vočadlo, L., 2015. The equation of state of the Pmmn phase of NiSi. J. Appl. Crystallogr. 48, 1914–1920. http://dx.doi.org/10.1107/S1600576715020087.

Lu, J., Gao, X., Zhang, S.-L., Hultman, L., 2013. Crystallization of $NiSi_x$ in a body-centered cubic structure during solid-state reaction between an ultrathin Ni film and Si(0 0 1) substrate at 150–350 °C. Cryst. Growth Des. 13, 1801–1806.

Malavergne, V., Toplis, M.J., Berthet, S., Jones, J., 2010. Highly reducing conditions during core formation on Mercury: implications for internal structure and the origin of a magnetic field. Icarus 206, 199–209.

Martorell, B., Brodholt, J., Wood, I.G., Vočadlo, L., 2013. The effect of nickel on the properties of iron at the conditions of Earth's inner core: ab initio calculations of seismic wave velocities of Fe-Ni alloys. Earth Planet. Sci. Lett. 365, 143–151.

Rivoldini, A., Van Hoolst, T., Verhoeven, O., 2009. The interior structure of Mercury and its core sulfur content. Icarus 201, 12–30.

Toby, B.H., 2001. EXPGUI, a graphical user interface for GSAS. J. Appl. Crystallogr. 34, 210–213.

Van Bockstael, C., De Keyser, K., Van Meirhaeghe, R.L., Detavernier, C., Jordan-Sweet, J., Lavoie, C., 2009. Influence of a transient hexagonal phase on the microstructure and morphological stability of NiSi films. Appl. Phys. Lett. 94, 033504.

Vočadlo, L., Wood, I.G., Dobson, D.P., 2012. High-pressure phase transitions and equations of state in NiSi I: an initio simulations. J. Appl. Crystallogr. 45, 186–196. http://dx.doi.org/10.1107/S0021889812000337.

Vočadlo, L., Price, G.D., Wood, I.G., 1999. Crystal structure, compressibility and possible phase transitions in ε-FeSi studied by first-principles pseudopotential calculations. Acta Crystallogr. A B55, 484–493.

Vočadlo, L., 2007. Ab initio calculations of the elasticity of iron alloys at inner core conditions: evidence for a partially molten inner core? Earth Planet. Sci. Lett. 254, 227–232.

Wood, I.G., Vočadlo, L., Knight, K.S., Dobson, D.P., Marshall, W.G., Price, G.D., Brodholt, J., 2004. Thermal expansion and crystal structure of cementite, Fe_3C, between 4 and 600 K determined by time-of-flight neutron powder diffraction. J. Appl. Crystallogr. 37, 82–90.

Wood, I.G., Ahmed, J., Dobson, D.P., Vočadlo, L., 2013. High-pressure phase transitions and equations of state in NiSi III: a new high-pressure phase of NiSi. J. Appl. Crystallogr. 46, 14–24.

Zhang, F., Oganov, A.R., 2010. Iron silicides at pressures of the Earth's inner core. Geophys. Res. Lett. 37. art. L02305.